

# Nonlinear Compact Finite-Difference Schemes with Semi-Implicit Time Stepping

Debojyoti Ghosh and Emil M. Constantinescu

**Abstract** Atmospheric flows are characterized by a large range of length scales as well as strong gradients. The accurate simulation of such flows requires numerical algorithms with high spectral resolution, as well as the ability to provide nonoscillatory solutions across regions of high gradients. These flows exhibit a large range of time scales as well—the slowest waves propagate at the flow velocity and the fastest waves propagate at the speed of sound. Time integration with explicit methods are thus inefficient, although algorithms with semi-implicit time integration have been used successfully in past studies. We propose a finite-difference method for atmospheric flows that uses a weighted compact scheme for spatial discretization and implicit-explicit additive Runge-Kutta methods for time integration. We present results for a benchmark atmospheric flow problem and compare our results with existing ones in the literature.

## 1 Introduction

The simulation of atmospheric flows requires accurate numerical solutions of the compressible Navier-Stokes equations or the inviscid Euler equations if the physical viscosity and heat conduction are neglected. Such flows are characterized by localized flow structures and strong gradients, and numerical algorithms need a high spectral resolution and must be nonoscillatory across regions of strong gradients. Algorithms used for numerical weather prediction include finite-difference methods [13], finite-volume methods [1], and discontinuous Galerkin and spectral element methods [10, 9]. Although standard finite-difference methods suffer from poor spectral resolution, compact finite-difference methods [15] have significantly

---

Debojyoti Ghosh  
Mathematics & Computer Science Division, Argonne National Laboratory, Argonne, IL, United States e-mail: ghosh@mcs.anl.gov

Emil M. Constantinescu  
Mathematics & Computer Science Division, Argonne National Laboratory, Argonne, IL, United States e-mail: emconsta@mcs.anl.gov

higher spectral resolution and have been applied to applications such as large eddy simulations and direct numerical simulations of turbulent flows [14, 18].

In this study, we propose a high-order finite-difference method for atmospheric flows based on compact-reconstruction weighted essentially nonoscillatory (CR-WENO) schemes [5, 6, 8]. The CRWENO schemes combine the high spectral resolution of linear compact schemes with the solution-dependent stencil adaptation method of the WENO schemes [17, 11] to produce nonoscillatory solutions. They are thus well suited for simulating atmospheric flows. We explore implicit-explicit time-integration schemes based on a separation of stiff and nonstiff components of the governing equations [10]. We present results for a benchmark atmospheric flow problem.

## 2 Governing Equations

We consider the conservative form of the Euler equations based on the mass, momentum, and potential temperature for mesoscale flows (neglecting the Coriolis forces) [10]. These are given by

$$\frac{\partial}{\partial t} \begin{bmatrix} \rho' \\ \rho \mathbf{u} \\ \rho \theta \end{bmatrix} + \nabla \cdot \begin{bmatrix} \rho \mathbf{u} \\ \rho \mathbf{u} \otimes \mathbf{u} + p' \mathcal{I} \\ \rho \theta \mathbf{u} \end{bmatrix} = \begin{bmatrix} 0 \\ -\rho' g \hat{\mathbf{k}} \\ 0 \end{bmatrix} \quad (1)$$

where  $\rho$  is the density,  $\mathbf{u}$  is the velocity vector,  $p$  is the pressure,  $\mathcal{I}$  is the identity matrix, and  $g$  is the acceleration due to gravity acting along the  $z$ -axis of the coordinate system with unit vector  $\hat{\mathbf{k}}$ . The potential temperature  $\theta$  is given by

$$\theta = \frac{T}{\pi}; \quad \pi = \left( \frac{p}{p_0} \right)^{\frac{R}{C_p}}, \quad (2)$$

where  $T$  is the temperature,  $\pi$  is the Exner pressure,  $p_0$  is the pressure at the surface (or reference altitude),  $R$  is the universal gas constant, and  $C_p$  is the constant pressure specific heat. The system of equations is completed by the equation of state,  $p = p_0 \left( \frac{\rho R \theta}{p_0} \right)^{\frac{C_p}{C_v}}$ , where  $C_v$  is the constant volume specific heat. Equation (1) is expressed in terms of the density, pressure, and potential temperature perturbations ( $\rho'$ ,  $p'$ ,  $\theta'$ ) that can be expressed as  $(\cdot)' = (\cdot)(x, y, z, t) - (\bar{\cdot})(z)$ , where  $(\bar{\cdot})$  is the mean density, pressure, or potential temperature in hydrostatic balance  $C_p \bar{\theta} \frac{d\bar{\pi}}{dz} = -g$ . The governing equations form a system of hyperbolic partial differential equations (PDEs) and are solved by a conservative finite-difference algorithm.

### 3 Numerical Methodology

Equation (1) can be expressed as a system of hyperbolic conservation laws with a source term

$$\frac{\partial \mathbf{U}}{\partial t} + \frac{\partial \mathbf{f}_i(\mathbf{U})}{\partial x_i} = \mathbf{s}(\mathbf{U}), \quad i = 1, \dots, D, \quad (3)$$

where  $\mathbf{U}$  is the solution,  $\mathbf{f}_i$  is the flux along the  $i$ th dimension,  $\mathbf{s}$  is the source term, and  $D$  is the number of dimensions. We describe the discretization of (3) in one dimension ( $D = 1$ ); it can be trivially extended to multiple dimensions. A conservative, finite-difference spatial discretization of (3) on this grid results in a semi-discrete ordinary differential equation (ODE) in time,

$$\frac{d\mathbf{U}_j}{dt} + \frac{1}{\Delta x} [\hat{\mathbf{f}}_{j+1/2} - \hat{\mathbf{f}}_{j-1/2}] = \mathbf{s}_j, \quad j = 1, \dots, N, \quad (4)$$

where  $j$  denotes the grid index,  $\mathbf{U}_j = \mathbf{U}(x_j)$  is the cell-centered solution,  $\hat{\mathbf{f}}_{j+1/2}$  is the numerical flux at the cell interface  $x_{j+1/2}$ , and  $\mathbf{s}_j$  is the source term evaluated at the cell center.

#### 3.1 Reconstruction

We use the CRWENO scheme [5, 6, 8] to reconstruct the interface fluxes  $\hat{\mathbf{f}}_{j+1/2}$  from the cell-centered flux  $\mathbf{f}_j$ . We briefly summarize the scheme in this section; a more complete description is available in [5]. The fifth-order CRWENO scheme (CRWENO5) is constructed by considering three third-order-accurate compact interpolation schemes for the flux function at the  $(j + 1/2)$ th interface:

$$\frac{2}{3}\hat{f}_{j-1/2} + \frac{1}{3}\hat{f}_{j+1/2} = \frac{1}{6}(f_{j-1} + 5f_j); \quad c_1 = \frac{2}{10}, \quad (5)$$

$$\frac{1}{3}\hat{f}_{j-1/2} + \frac{2}{3}\hat{f}_{j+1/2} = \frac{1}{6}(5f_j + f_{j+1}); \quad c_2 = \frac{5}{10}, \quad (6)$$

$$\frac{2}{3}\hat{f}_{j+1/2} + \frac{1}{3}\hat{f}_{j+3/2} = \frac{1}{6}(f_j + 5f_{j+1}); \quad c_3 = \frac{3}{10}. \quad (7)$$

Multiplying (5)–(7) with their optimal coefficients ( $c_k$ ,  $k = 1, 2, 3$ ) and adding, we obtain the fifth-order-accurate compact interpolation scheme,

$$\frac{3}{10}\hat{f}_{j-1/2} + \frac{6}{10}\hat{f}_{j+1/2} + \frac{1}{10}\hat{f}_{j+3/2} = \frac{1}{30}f_{j-1} + \frac{19}{30}f_j + \frac{1}{3}f_{j+1}. \quad (8)$$

We now compute weights  $\omega_k$  based on the local smoothness of the solution [11] such that they converge to the corresponding optimal coefficient  $c_k$  when the solution is locally smooth, and approach zero at or near a discontinuity. They can be expressed as

$$\omega_k = \frac{\alpha_k}{\sum_k \alpha_k}; \quad \alpha_k = \frac{c_k}{(\varepsilon + \beta_k)^p}; \quad k = 1, 2, 3, \quad (9)$$

where  $\varepsilon = 10^{-6}$  is a small number to prevent division by zero. The smoothness indicators ( $\beta_k$ ) measure the local smoothness of the solution and are given by

$$\beta_1 = \frac{13}{12}(f_{j-2} - 2f_{j-1} + f_j)^2 + \frac{1}{4}(f_{j-2} - 4f_{j-1} + 3f_j)^2, \quad (10)$$

$$\beta_2 = \frac{13}{12}(f_{j-1} - 2f_j + f_{j+1})^2 + \frac{1}{4}(f_{j-1} - f_{j+1})^2, \quad (11)$$

$$\text{and } \beta_3 = \frac{13}{12}(f_j - 2f_{j+1} + f_{j+2})^2 + \frac{1}{4}(3f_j - 4f_{j+1} + f_{j+2})^2. \quad (12)$$

Multiplying (5)–(7) with  $\omega_k$  instead of  $c_k$ , and adding, we obtain the CRWENO5 scheme:

$$\begin{aligned} & \left( \frac{2}{3}\omega_1 + \frac{1}{3}\omega_2 \right) \hat{f}_{j-1/2} + \left[ \frac{1}{3}\omega_1 + \frac{2}{3}(\omega_2 + \omega_3) \right] \hat{f}_{j+1/2} + \frac{1}{3}\omega_3 \hat{f}_{j+3/2} \\ & = \frac{\omega_1}{6} f_{j-1} + \frac{5(\omega_1 + \omega_2) + \omega_3}{6} f_j + \frac{\omega_2 + 5\omega_3}{6} f_{j+1}. \end{aligned} \quad (13)$$

This scheme is fifth-order accurate when the solution ( $\omega_k \rightarrow c_k$ ) is smooth, and it yields a nonoscillatory solution across discontinuities by biasing the interpolation stencil away from it. Equation (13) requires the solution to a tridiagonal system of equations at each time-integration step or stage; however, past studies [5] demonstrated the higher computational efficiency of the CRWENO scheme compared with a standard finite-difference scheme. A scalable and efficient parallel implementation of the CRWENO5 scheme is discussed in [7]. This discussion describes the left-biased computation of the interface flux; the corresponding expressions for the right-biased interface flux can be similarly obtained. The final flux at a given interface is computed from the left- and right-biased approximations by using the Rusanov upwinding scheme [16].

### 3.2 Time Integration

Equation (4) is integrated in time by using explicit Runge-Kutta (ERK) and implicit-explicit additive Runge-Kutta (ARKIMEX) methods. Efficient implementations of these methods are available in the `TS` (time-stepping) module of `PETSC` [3, 4]. ERK methods are often inefficient, however, because the time-step size is restricted by the acoustic (fastest) wave. Implicit-explicit time-integration methods have been previously applied to atmospheric flows [10, 9]. We briefly summarize the separation of stiff and nonstiff components of the governing equations and its implicit-explicit discretization in time.

Equation (1) can be rearranged such that the right-hand side comprises a nonstiff term and a linear stiff term [10],

$$\frac{\partial \mathbf{U}}{\partial t} = \mathbf{S}(\mathbf{U}) + \mathbf{L}(\mathbf{U}), \quad (14)$$

$$\mathbf{U} = \begin{bmatrix} \rho' \\ \rho \mathbf{u} \\ \rho \theta' \end{bmatrix}, \quad \mathbf{S}(\mathbf{u}) = -\nabla \cdot \begin{bmatrix} 0 \\ \rho \mathbf{u} \otimes \mathbf{u} \\ \rho \theta \mathbf{u} - \rho \bar{\theta} \mathbf{u} \end{bmatrix}, \quad \mathbf{L}(\mathbf{u}) = - \begin{bmatrix} \nabla \cdot \rho \mathbf{u} \\ \nabla p' + g \rho' \hat{\mathbf{k}} \\ \nabla \cdot \rho \bar{\theta} \mathbf{u} \end{bmatrix},$$

where the pressure perturbation is linearized as  $p' = \frac{\gamma \bar{p}}{\bar{\rho} \bar{\theta}} (\rho \theta - \bar{\rho} \bar{\theta})$ , with  $\gamma = C_P/C_V$  as the specific heat ratio. The nonstiff component,  $\mathbf{S}(\mathbf{U})$ , of the right-hand side of (14) consists of the entropy waves; and the linear stiff component,  $\mathbf{L}(\mathbf{U})$ , consists of the acoustic and gravity waves. Equation (14) is spatially discretized and integrated in time by using the ARKIMEX methods [2, 12, 19], where an ERK method is applied to the nonstiff term and an ARK method is applied to the stiff term. This multistage procedure can be expressed as

$$\mathbf{U}^{(k)} = \mathbf{U}_n + \Delta t \sum_{i=1}^{k-1} a_{ki} \hat{\mathbf{S}}(\mathbf{U}^{(i)}) + \Delta t \sum_{i=1}^k \tilde{a}_{ki} \hat{\mathbf{L}}(\mathbf{U}^{(i)}), \quad k = 1, \dots, s, \quad (15)$$

$$\mathbf{U}_{n+1} = \mathbf{U}_n + \Delta t \sum_{i=1}^s b_i \hat{\mathbf{S}}(\mathbf{U}^{(i)}) + \Delta t \sum_{i=1}^s \tilde{b}_i \hat{\mathbf{L}}(\mathbf{U}^{(i)}), \quad (16)$$

where  $s$  is the number of stages, the superscripts of  $\mathbf{U}$  indicate the stage index, and the subscripts of  $\mathbf{U}$  indicate the time step. The coefficients  $a_{ki}$  and  $b_i$  specify the ERK method, and the coefficients  $\tilde{a}_{ki}$  and  $\tilde{b}_i$  specify the ARK method.  $\hat{\mathbf{S}}$  and  $\hat{\mathbf{L}}$  are the spatially discretized forms of  $\mathbf{S}(\mathbf{U})$  and  $\mathbf{L}(\mathbf{U})$ , respectively.

Past applications of implicit-explicit time-integration to atmospheric flows [10, 9] used discontinuous Galerkin or spectral element methods for the discretization of spatial derivatives; these approaches resulted in (15) being a linear system. We, however, use a nonlinear finite-difference operator to discretize the spatial derivative, as given by (4) and (13). Thus,  $\hat{\mathbf{L}}$  is nonlinear even though  $\mathbf{L}$  is linear, and (15) is a nonlinear system of equations. We make two comments on our algorithm in this context.

- We ensure that the discretized right-hand side ( $\hat{\mathbf{S}} + \hat{\mathbf{L}}$ ) is consistent with the right-hand side of (14) by using the *same* finite-difference operator to discretize both  $\mathbf{S}$  and  $\mathbf{L}$ . The nonlinear weights in (13) are computed based on the smoothness of  $\mathbf{S} + \mathbf{L}$ , and the resulting CRWENO5 scheme is applied to both terms.
- We linearize the finite-difference operator at each stage such that (15) is a linear system of equations. We compute the nonlinear weights in (13) at the beginning of stage  $k$  based on the smoothness of  $(\mathbf{S} + \mathbf{L})(\mathbf{U}^{(k-1)})$  (or  $(\mathbf{S} + \mathbf{L})(\mathbf{U}_n)$  for  $k = 1$ ); and we solve (15) as a linear system (since, once the nonlinear weights are fixed, (13) is a linear operator).

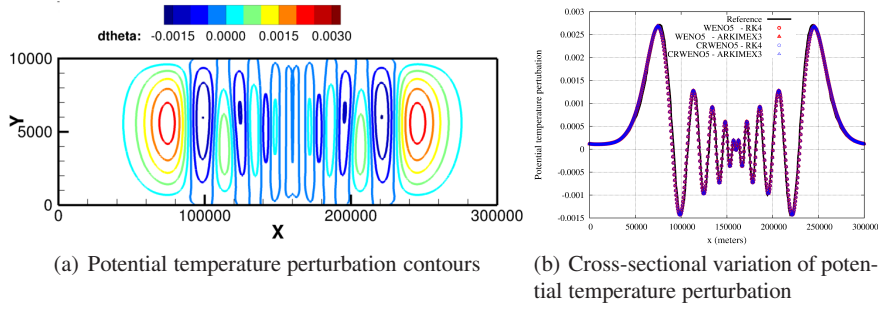


**Fig. 1** Solutions of the inertia-gravity wave problem obtained on a grid with  $1200 \times 50$  points.

## 4 Results

We verify our algorithm by solving the two-dimensional inertia-gravity wave problem, a benchmark atmospheric flow problem [13]. The domain is a periodic channel with dimensions  $300,000 \times 10,000$  meters. Zero-flux boundary conditions are specified at the top and bottom boundaries. The initial atmosphere has a mean flow of 20 meters/second and is uniformly stratified with a Brunt-Vaisala frequency of  $\mathcal{N} = 0.01/\text{second}$  [10, 13]. A perturbation in the potential temperature is introduced as

$$\theta' = \theta_c \frac{\sin\left(\frac{\pi_c z}{h_c}\right)}{1 + \left(\frac{x-x_c}{a_c}\right)^2}, \quad (17)$$

where  $\theta_c = 0.01$  Kelvin,  $h_c = 10,000$  meters,  $a_c = 5000$  meters,  $x_c = 100,000$  meters, and  $\pi_c$  is the trigonometric constant. Solutions are obtained at a final time of 3000 seconds.

Figure 1(a) shows the potential temperature perturbation ( $\theta'$ ) contours for a solution obtained with the CRWENO5 scheme on a grid with  $1200 \times 50$  points. The solution is integrated in time with the second-order-accurate, two-stage ARKIMEX 2C method at a CFL of 8. We observe good agreement with results in the literature [1, 10, 13]. The cross-sectional variation of the potential temperature perturbation through  $z = 5000$  meters is shown in Figure 1(b) for the solutions obtained with the CRWENO5 as well as the fifth-order WENO (WENO5) [11] schemes. The explicit four-stage, fourth-order Runge-Kutta (RK4) and the three-stage, third-order ARKIMEX (ARKIMEX3) methods are used to integrate the solution in time. Excellent agreement is observed for all the methods with the reference solution, obtained by using the spectral element method with 10th-order polynomials and 250-meter grid resolution [10].

The convergence and conservation properties of our algorithm are evaluated by obtaining solutions on a fine grid with  $8192 \times 256$  points. Figure 2(a) shows the  $L_2$  norm of the error as a function of the time-step sizes. The reference solution

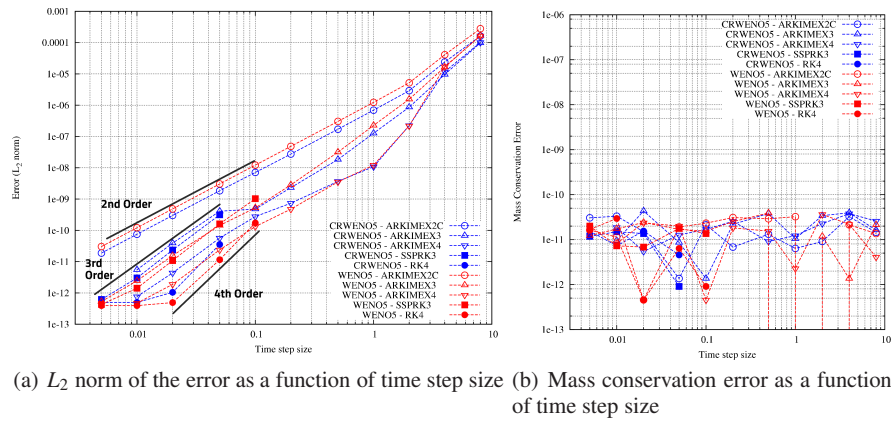


**Fig. 2** Error analysis on a grid with  $8192 \times 256$  points.

is computed with the strong-stability-preserving three-stage, third-order Runge-Kutta (SSPRK3) scheme and a small time-step size of 0.0005. We consider two ERK schemes, SSPRK3 and RK4, and three ARKIMEX schemes, ARKIMEX2C, ARKIMEX3, and ARKIMEX4 (four-stage, fourth-order). The methods converge at their theoretical convergence rates. Figure 2(b) shows the error in mass conservation for the various methods and time-step sizes. Mass is conserved to round-off error for all the methods considered.

## 5 Conclusions

A high-order-accurate finite-difference method for the simulation of atmospheric flows is proposed in this paper. The algorithm uses the CRWENO scheme for spatial discretization and the ARKIMEX schemes for time integration. The high spectral resolution of the CRWENO scheme allows the accurate modeling of all relevant length scales, while maintaining nonoscillatory behavior across regions of strong gradients. The ARKIMEX methods split the governing equations into its stiff and nonstiff components and integrates them with implicit and explicit multistage Runge-Kutta schemes, respectively. Thus, the time-step size is not restricted by the acoustic waves. The algorithm is applied to a benchmark atmospheric flow problem, and solutions show excellent agreement with existing results in the literature. The split implicit-explicit time-integrators show optimal convergence when coupled with the nonlinear finite-difference scheme and do not violate mass conservation.

**Acknowledgements** This material is based upon work supported by the U.S. Department of Energy, Office of Science, Advanced Scientific Computing Research, under contract DE-AC02-06CH11357.

## References

1. Ahmad, N., Lindeman, J.: Euler solutions using flux-based wave decomposition. *International Journal for Numerical Methods in Fluids* **54**(1), 47–72 (2007). DOI 10.1002/flid.1392
2. Ascher, U.M., Ruuth, S.J., Spiteri, R.J.: Implicit-explicit Runge-Kutta methods for time-dependent partial differential equations. *Applied Numerical Mathematics* **25**(2-3), 151–167 (1997). DOI 10.1016/S0168-9274(97)00056-1
3. Balay, S., Brown, J., Buschelman, K., Eijkhout, V., Gropp, W.D., Kaushik, D., Knepley, M.G., McInnes, L.C., Smith, B.F., Zhang, H.: PETSc Users Manual. Tech. Rep. ANL-95/11 - Revision 3.4, Argonne National Laboratory (2013)
4. Balay, S., Brown, J., Buschelman, K., Gropp, W.D., Kaushik, D., Knepley, M.G., McInnes, L.C., Smith, B.F., Zhang, H.: PETSc Web page (2013). <http://www.mcs.anl.gov/petsc>
5. Ghosh, D., Baeder, J.D.: Compact reconstruction schemes with weighted ENO limiting for hyperbolic conservation laws. *SIAM Journal on Scientific Computing* **34**(3), A1678–A1706 (2012). DOI 10.1137/110857659
6. Ghosh, D., Baeder, J.D.: Weighted non-linear compact schemes for the direct numerical simulation of compressible, turbulent flows. *Journal of Scientific Computing* **61**(1), 61–89 (2014). DOI 10.1007/s10915-014-9818-0
7. Ghosh, D., Constantinescu, E.M., Brown, J.: Efficient implementation of nonlinear compact schemes on massively parallel platforms. Submitted
8. Ghosh, D., Medida, S., Baeder, J.D.: Application of compact-reconstruction weighted essentially nonoscillatory schemes to compressible aerodynamic flows. *AIAA Journal* **52**(9), 1858–1870 (2014). DOI 10.2514/1.J052654
9. Giraldo, F., Kelly, J., Constantinescu, E.: Implicit-explicit formulations of a three-dimensional nonhydrostatic unified model of the atmosphere (NUMA). *SIAM Journal on Scientific Computing* **35**(5) (2013). DOI 10.1137/120876034
10. Giraldo, F., Restelli, M., Läuter, M.: Semi-implicit formulations of the Navier-Stokes equations: Application to nonhydrostatic atmospheric modeling. *SIAM Journal on Scientific Computing* **32**(6), 3394–3425 (2010). DOI 10.1137/090775889
11. Jiang, G.S., Shu, C.W.: Efficient implementation of weighted ENO schemes. *Journal of Computational Physics* **126**(1), 202–228 (1996). DOI 10.1006/jcph.1996.0130
12. Kennedy, C.A., Carpenter, M.H.: Additive Runge-Kutta schemes for convection-diffusion-reaction equations. *Applied Numerical Mathematics* **44**(1-2), 139–181 (2003). DOI 10.1016/S0168-9274(02)00138-1
13. Klemp, J.B., Skamarock, W.C., Dudhia, J.: Conservative split-explicit time integration methods for the compressible nonhydrostatic equations. *Monthly Weather Review* **135**, 28972913 (2007). DOI 10.1175/MWR3440.1
14. Lee, C., Seo, Y.: A new compact spectral scheme for turbulence simulations. *Journal of Computational Physics* **183**(2), 438–469 (2002). DOI 10.1006/jcph.2002.7201
15. Lele, S.K.: Compact finite difference schemes with spectral-like resolution. *Journal of Computational Physics* **103**(1), 16–42 (1992). DOI 10.1016/0021-9991(92)90324-R
16. LeVeque, R.J.: *Finite Volume Methods for Hyperbolic Problems*. Cambridge Texts in Applied Mathematics. Cambridge University Press (2002)
17. Liu, X.D., Osher, S., Chan, T.: Weighted essentially non-oscillatory schemes. *Journal of Computational Physics* **115**(1), 200–212 (1994). DOI 10.1006/jcph.1994.1187
18. Nagarajan, S., Lele, S.K., Ferziger, J.H.: A robust high-order compact method for large eddy simulation. *Journal of Computational Physics* **191**(2), 392–419 (2003). DOI 10.1016/S0021-9991(03)00322-X
19. Pareschi, L., Russo, G.: Implicit-explicit Runge-Kutta schemes and applications to hyperbolic systems with relaxation. *Journal of Scientific Computing* **25**(1-2), 129–155 (2005). DOI 10.1007/BF02728986



Government License The submitted manuscript has been created by UChicago Argonne, LLC, Operator of Argonne National Laboratory ("Argonne"). Argonne, a U.S. Department of Energy Office of Science laboratory, is operated under Contract No. DE-AC02-06CH11357. The U.S. Government retains for itself, and others acting on its behalf, a paid-up nonexclusive, irrevocable worldwide license in said article to reproduce, prepare derivative works, distribute copies to the public, and perform publicly and display publicly, by or on behalf of the Government.